


RESEARCH ARTICLE

Carbon-13 chemical shift tensor measurements for nitrogen-dense compounds

Sean T. Holmes^{1,2} | Cameron M. Boley³ | Angelika Dewicki³ |
 Zachary T. Gardner³ | Cameron S. Vojvodin^{1,2} | Robbie J. Iulucci³ |
 Robert W. Schurko^{1,2} 

¹Department of Chemistry & Biochemistry, Florida State University, Tallahassee, Florida, USA

²National High Magnetic Field Laboratory, Tallahassee, Florida, USA

³Department of Chemistry, Washington and Jefferson College, Washington, Pennsylvania, USA

Correspondence

Robert W. Schurko, Department of Chemistry & Biochemistry, Florida State University, Tallahassee, FL 32306, USA.
 Email: rschurko@fsu.edu

Robbie J. Iulucci, Department of Chemistry, Washington and Jefferson College, Washington, PA 15301, USA.
 Email: riulucci@washjeff.edu

Funding information

Florida State University; National High Magnetic Field Laboratory; National Science Foundation Cooperative Agreement, Grant/Award Numbers: DMR-2128556, DMR-1644779; State of Florida. R.J.I., Grant/Award Numbers: REU CHE-1950585, MRI CHE-1726824; FSU Department of Chemistry and Biochemistry, Grant/Award Number: FSU075000XRAY

Abstract

This paper reports the principal values of the ¹³C chemical shift tensors for five nitrogen-dense compounds (i.e., cytosine, uracil, imidazole, guanidine hydrochloride, and aminoguanidine hydrochloride). Although these are all fundamentally important compounds, the majority do not have ¹³C chemical shift tensors reported in the literature. The chemical shift tensors are obtained from ¹H→¹³C cross-polarization magic-angle spinning (CP/MAS) experiments that were conducted at a high field of 18.8 T to suppress the effects of ¹⁴N-¹³C residual dipolar coupling. Quantum chemical calculations using density functional theory are used to obtain the ¹³C magnetic shielding tensors for these compounds. The best agreement with experiment arises from calculations using the hybrid functional PBE0 or the double-hybrid functional PBE0-DH, along with the triple-zeta basis sets TZ2P or pc-3, respectively, and intermolecular effects modeled using large clusters of molecules with electrostatic embedding through the COSMO approach. These measurements are part of an ongoing effort to expand the catalog of accurate ¹³C chemical shift tensor measurements, with the aim of creating a database that may be useful for benchmarking the accuracy of quantum chemical calculations, developing nuclear magnetic resonance (NMR) crystallography protocols, or aiding in applications involving machine learning or data mining. This work was conducted at the National High Magnetic Field Laboratory as part of a 2-week school for introducing undergraduate students to practical laboratory experience that will prepare them for scientific careers or postgraduate studies.

KEYWORDS

carbon, chemical shift, database, DFT, NMR, NMR crystallography

Cameron M. Boley, Angelika Dewicki, and Zachary T. Gardner made equal contributions as part of the inaugural MagLab Winter NMR School.

1 | INTRODUCTION

Nuclear magnetic resonance (NMR) chemical shifts are among the most sensitive spectroscopic parameters to differences and/or changes in molecular-level structure.¹ In the solid state, measurement of the symmetric second-rank tensor that describes the chemical shift provides a detailed description of the electronic environment surrounding the atomic nucleus. While measurement of the orientation of the chemical shift tensor in the molecular frame (or the six principal values within the icosahedral representation of the chemical shift tensor)² requires both a crystal of suitable size and quality and specialized single-crystal NMR probes and measurements,^{3–5} the three principal values of the tensor can be extracted by fitting solid-state NMR (SSNMR) spectra from studies on powder samples (high-resolution magic-angle spinning [MAS] is by far the most common technique, although measurements can also be made on stationary samples).⁶ Thus, measurement of the principal values of the chemical shift tensors for powder samples has far reaching applications, including the validation, refinement, and de novo determination of crystal structures, which is the focus of the field of NMR crystallography.^{7–11}

To aid NMR crystallographic investigations involving quantum chemical calculations,^{12–25} NMR-guided crystal structure prediction,^{26–28} NMR-guided Rietveld refinements of crystal structures,^{29–35} machine learning,^{36–39} and data-driven approaches,⁴⁰ a comprehensive database containing chemical shift tensors and corresponding crystal structures would prove invaluable. Such a database would be composed of accurately measured principal values of chemical shift tensors for important chemical compounds with well-defined crystal structures and should adequately represent the diversity of chemical environments found in nature. There are several benchmarking studies that have compiled lists of ¹³C chemical shift tensors and provided density functional theory (DFT) calculations of their magnetic shielding tensors, using X-ray and/or neutron diffraction data as structural models. Johnston et al. modeled the full ¹³C chemical shift tensors for a series of saccharides and aromatic molecules that have been characterized by single-crystal NMR and neutron diffraction, because these types of molecules were the focus of the pioneering research of David M. Grant and coworkers.¹² By focusing only on principal values of tensors, Holmes et al. examined a more comprehensive and diverse set of molecular crystals including those materials listed above, as well as several amino acids, pharmaceuticals, and other relevant organic molecules.¹³ However, the latter database still contains relatively few examples of carbon atoms bonded directly to nitrogen, being mostly limited to amino acids. This is a

surprising fact, especially when one considers the frequency with which nitrogen is found in active pharmaceutical ingredients (APIs) and molecules of biological importance such as peptides, proteins, and nucleotides. These facts drive the need to expand the ¹³C chemical shift tensor database to include a larger number of nitrogen-dense organic compounds.

Because some ¹³C magnetic shielding tensors have a strong dependence on the extended crystal lattice environment, three general methods have evolved to calculate magnetic shielding tensors in crystalline solids using DFT. The first approach is exemplified by the gauge including projector augmented wave (GIPAW) method,^{25,41} which is capable of predicting magnetic shielding tensors in crystals through a combination of plane-wave basis sets, core-valence interactions modeled using pseudopotentials, and periodic boundary conditions that account for lattice interactions. An alternate approach is the execution of DFT calculations on models featuring large clusters of molecules that represent a local region of the crystal structure, without use of periodic boundary conditions.^{13–16} Similarly, fragment-based approaches allow intermolecular interactions to be modeled piecewise with each calculation accounting for a subset of possible interactions, and the summation of the results of these calculations providing the magnetic shielding tensor.^{18,19,21} Additional considerations for cluster- and fragment-based approaches include (i) the potential to perform calculations using levels of theory that are currently untenable with plane waves—these options include the use of hybrid and double-hybrid functionals, as well relativistic corrections at the spin-orbit level (for systems containing heavy atoms); (ii) electrostatic embedding to mimic interactions with more distant molecules^{17,42}; and (iii) monomer^{20,22,23,43} and/or fragment corrections²⁰ that allow calculations on a single molecule (or small cluster of molecules) to be performed using methods that would be prohibitively expensive if performed using a full cluster, potentially leading to better agreement with experiment.

When sufficiently robust computational protocols are used, the principal values of the ¹³C chemical shift tensor (as defined by the chemical shift distance, d_v , for atom v , or the RMS chemical shift distance, Δ_{RMS} , for multiple atoms²; see Supporting Information S1) can be calculated within ± 3 ppm of experimental values. However, recent work indicates that the values of d_v and/or Δ_{RMS} are larger for carbon atoms found in moieties containing nitrogen¹⁶; at present, it is not clear whether these differences between calculation and experiment reflect deficiencies in the quantum chemical calculations (which may be anticipated to affect the shifts of all types of carbon atoms within the same moiety as the nitrogen atom) or experimental

uncertainties of the chemical shift tensors of such carbon atoms (which would be expected to have an impact only for carbon atoms bound to nitrogen, *vide infra*).

The measurement of ^{13}C chemical-shift tensors for nitrogen-dense compounds is challenging, in part because the effects of ^{14}N - ^{13}C residual dipolar coupling cannot be completely averaged by MAS (i.e., residual dipolar coupling does not follow the familiar $3\cos^2\theta - 1$ geometry dependence), leading to broadening and/or splitting of ^{13}C peaks.^{44–47} In turn, this interferes with the determination of ^{13}C chemical shift tensors when using methods based on relative intensities of the peaks (e.g., Herzfeld–Berger analysis). In some cases, the measurement of chemical shift tensors can be aided using prior knowledge of the quadrupolar coupling constant and asymmetry parameter describing the electric field gradient (EFG) tensor of the nitrogen atom, as well as the orientation of the EFG tensor in the molecular frame. However, a more straightforward solution is to perform the measurements using high magnetic fields because doing so reduces the splitting of ^{13}C peaks due to the ^{14}N - ^{13}C residual dipolar coupling and simplifies the effects of the interaction to line broadening.

Herein, we report the ^{13}C chemical shift tensors for a series of nitrogen-dense compounds, including imidazole, uracil, cytosine, guanidine HCl, and aminoguanidine HCl. With the exception of uracil,⁴⁸ the ^{13}C chemical shift tensors for these important compounds have not been reported. To overcome challenges associated with ^{14}N - ^{13}C residual dipolar coupling, all spectra are measured at 18.8 T at the National High Magnetic Field Laboratory (MagLab) using $^1\text{H}\rightarrow^{13}\text{C}$ cross-polarization magic-angle spinning (CP/MAS) techniques. Because of the relative simplicity of the high-field ^{13}C spectra, baseline resolution of the spinning sidebands was achieved without resorting to multidimensional techniques, allowing the principal components of the ^{13}C chemical shift tensors to be extracted by analysis of the sideband manifold of the MAS spectra. This research was undertaken during the inaugural MagLab Winter NMR School in January 2023; this 2-week program is meant to introduce students from primarily undergraduate institutions to practical laboratory experience to prepare them for scientific careers or postgraduate studies.

2 | EXPERIMENTAL AND COMPUTATIONAL METHODS

2.1 | Materials

All materials were purchased from MilliporeSigma and used without further purification. Their identities

and purities were verified through powder X-ray diffraction (PXRD) and comparison with simulated PXRD patterns based on the known crystal structures.^{49–53}

2.2 | PXRD

PXRD patterns were acquired using a Rigaku MiniFlex benchtop diffractometer with a $\text{Cu K}\alpha$ radiation source and a D/teX Ultra2 detector. Samples were packed on zero-background silicon wafers with a well size of 5.0×0.2 mm. Experiments were conducted with an X-ray voltage of 40 kV, a current of 20 mA, 2θ angles over the range of $5\text{--}50^\circ$, a step size of 0.03° , and a dwell time of 5 s.

2.3 | SSNMR spectroscopy

SSNMR spectra were acquired at the National High Magnetic Field Laboratory in Tallahassee, FL. Spectra were acquired at 18.8 T using a medium-bore Oxford magnet and a Bruker Avance III HD console for which $\nu_0(^1\text{H}) = 800.12$ MHz and $\nu_0(^{13}\text{C}) = 201.22$ MHz. Experiments were conducted using a home-built 3.2-mm low-E HXY MAS probe⁵⁴ with samples packed into 3.2-mm o.d. zirconia rotors. A $^1\text{H}\rightarrow^{13}\text{C}$ ramped-amplitude CP/MAS sequence was used to acquire the ^{13}C SSNMR spectra.^{55–59} The experiments used a ^1H $\pi/2$ pulse of 3.33 μs , SPINAL-64 ^1H decoupling⁶⁰ with $\nu_2 = 75$ kHz, a spinning rate between $\nu_{\text{rot}} = 3.5$ and 10.0 kHz, contact times of 4.0 ms with a Hartmann–Hahn matching field⁶¹ of 50 kHz (matched on the X channel), and optimized recycle delays ranging between 3 and 10 min. Chemical shifts were referenced to neat TMS at $\delta_{\text{iso}}(^{13}\text{C}) = 0.0$ ppm using the high-frequency peak of α -glycine at $\delta_{\text{iso}}(^{13}\text{C}) = 176.5$ ppm as a secondary reference.^{62,63} Acquisition parameters for all experiments are found in the Supporting Information (Table S1).

All spectra were processed using TopSpin v.4.1.4 and fit using ssNake v.1.3.⁶⁴ Estimates of the uncertainties in the principal components of the ^{13}C chemical shift tensors were assessed using the HBA software package.⁶⁵ Numerical simulations of the influence of ^{14}N - ^{13}C residual dipolar coupling on the ^{13}C line shapes were conducted using WSOLIDS1.⁶⁶

2.4 | Computational methods

2.4.1 | Geometry optimizations

Plane-wave DFT geometry optimizations were performed using the CASTEP module within BIOVIA Materials

Studio 2020.⁶⁷ Previously reported crystal structures were used as starting structural models (Table S2).^{49–53} These calculations used the RPBE functional,⁶⁸ ultrasoft pseudopotentials generated *on-the-fly*,⁶⁹ a plane-wave cutoff energy of 800 eV, and a Monkhorst–Pack grid with a k -point spacing of 0.05 \AA^{-1} .⁷⁰ Dispersion corrections were introduced using the semiempirical two-body dispersion force field correction of Grimme.⁷¹ Structural refinements employed the LBFSGS energy-minimizing scheme,⁷² in which the positions of all atoms were relaxed while holding unit cell parameters constant, with convergence thresholds including a maximum change in energy of $5 \times 10^{-6} \text{ eV atom}^{-1}$, a maximum displacement of $5 \times 10^{-4} \text{ \AA atom}^{-1}$, and a maximum Cartesian force of $10^{-2} \text{ eV \AA}^{-1}$.

2.4.2 | Magnetic shielding tensors

¹³C magnetic shielding tensors were calculated using the Materials Studio 2020, Amsterdam Modelling Suite (AMS 2022), or ORCA 5.0 software packages. Calculations of magnetic shielding tensors within Materials Studio employed the GIPAW method, whereas those in AMS and ORCA employed the GIAO method.^{73,74} All calculations were based on structural models resulting from geometry optimizations. CASTEP calculations used structural models consisting of the fully periodic crystal structures, which inherently account for lattice contributions to the magnetic shielding tensors. These calculations employed the RPBE functional,⁶⁸ ultrasoft pseudopotentials generated *on-the-fly*,⁶⁹ a plane-wave cutoff energy of 800 eV, and a k -point spacing of 0.05 \AA^{-1} .⁷⁰ ¹⁴N EFG tensors were calculated at the same level of theory. In contrast, calculations using AMS or ORCA used isolated molecules or large cluster of molecules as structural models, as outlined below.

¹³C magnetic shielding tensors were computed in AMS using large clusters consisting of 15 molecules (and chloride ions where appropriate) as structural models, as described in previous work^{13–16}; these clusters are illustrated in Figure S1. These calculations used either the RPBE⁶⁸ or hybrid PBE0 functionals.⁷⁵ A basis set partitioning scheme was applied in which the central molecule within the cluster was assigned the TZ2P basis set with Becke integration set to “excellent,”^{76,77} whereas all other molecules in the cluster were assigned the DZ basis set with “normal” Becke integration. ¹³C magnetic shielding tensors are calculated only for the central molecule within the cluster. The clusters for cytosine, uracil, and imidazole had neutral charges, whereas guanidine HCl and aminoguanidine HCl had net charges of +8 and +6, respectively. Electrostatic embedding was accomplished

through the conductor-like screening model (COSMO),^{78–81} as implemented in ADF.⁸² Water was chosen as the solvent, using Delley-type cavity construction,⁸³ with atomic cavity radii based on the van der Waals radii of Allinger.⁸⁴

Additional calculations of ¹³C magnetic shielding tensors were performed using a combination of the AMS and ORCA software packages. These calculations employed the double-hybrid functional PBE0-DH,⁸⁵ along with the Gaussian-type polarization-consistent basis set pc-3,⁸⁶ or the PBE0 functional⁷⁵ combined with the Slater-type basis set TZ2P. The magnetic shielding tensors were obtained from the results of three separate types of calculations: (i) a PBE0 calculation in AMS using the molecular clusters as structural models, along with electrostatic embedding provided by the COSMO approach; (ii) a PBE0 calculation in AMS using only an isolated molecule as a structural model; and (iii) a final PBE0-DH calculation in ORCA using an isolated molecule as the structural model. The first two calculations provide an intermolecular correction to the magnetic shielding tensor, whereas the third is a high-level calculation of the magnetic shielding tensor of a molecule in isolation; these contributions are coadded, and the resulting tensor is diagonalized to yield the principal values.^{20,22,23,43}

3 | RESULTS AND DISCUSSION

The crystallographic information for the nitrogen-dense compounds selected for this study (guanidine HCl, aminoguanidine HCl, uracil, cytosine, and imidazole) are listed in Table S2, with their molecular structures and atomic labeling shown in Scheme 1.^{49–53} The identities and purities of the commercially purchased powder samples were confirmed by PXRD and comparison with simulated patterns based on the known crystal structures (Figure S2).^{49–53} These results indicate that each material consists of a single polymorph, with no additional phases or impurities evident.

CASTEP geometry optimizations and subsequent calculations of ¹⁴N EFG tensors were used to assess the anticipated effects of ¹⁴N-¹³C residual dipolar coupling on the ¹³C line shapes in these nitrogen-dense materials. Numerical simulations of ¹³C line shapes conducted using WSOLIDS1 account for the following factors: (i) the ¹⁴N-¹³C dipolar coupling constants determined from the C-N bond lengths, (ii) the calculated ¹⁴N EFG tensors, and (iii) the polar angle β and azimuth angle α of the dipolar vector in the principal axis system of the ¹⁴N EFG tensor. Simulations were conducted for representative carbon sites considered in this work at fields between

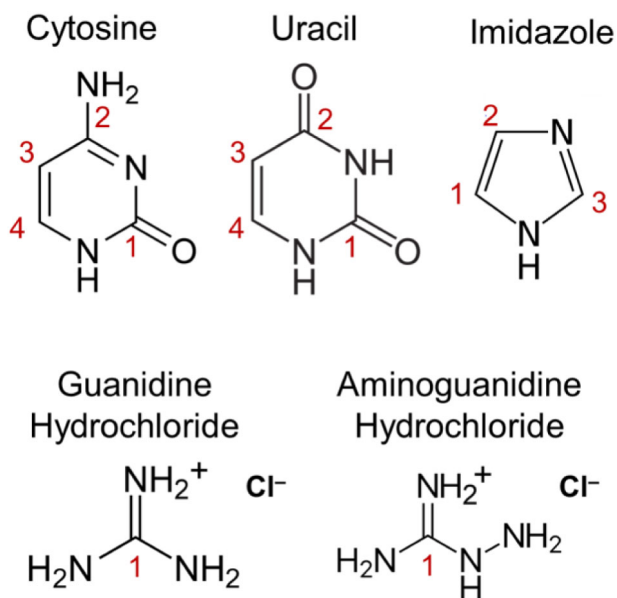
4.7 and 18.8 T (Figure S3). From these simulations, it was concluded that measurements at 18.8 T are sufficient to suppress the effects of ^{14}N - ^{13}C residual dipolar coupling.

Careful consideration of experimental conditions was necessary for acquiring high quality ^1H - ^{13}C CP/MAS SSNMR spectra, from which reliable ^{13}C chemical shift tensor principal values could be extracted. The Hartmann-Hahn matching conditions were established over the MAS frequency range from $\nu_{\text{rot}} = 3.5$ to 10.0 kHz using a ^{13}C -labeled sample of glycine (alpha polymorph) as a setup standard. Contact times and recycle delays for each subsequent sample were optimized using an MAS rate of $\nu_{\text{rot}} = 10.0$ kHz. However, slow

MAS spectra, from which the principal values of the ^{13}C chemical shift tensors can be derived, were obtained with MAS rates between $\nu_{\text{rot}} = 3.5$ and 6.0 kHz. Spinning speeds were selected to ensure the observation of at least three sidebands per side of the isotropic peak, while also minimizing overlap between peaks. Significantly, each compound featured a long value of $T_1(^1\text{H})$, resulting in recycle delays ranging between 3 and 10 min, and total experimental times between 19 and 43 h.

Each ^1H - ^{13}C CP/MAS spectrum features between one and four isotropic chemical shifts, all of which are consistent with the crystal structures that have a single crystallographically distinct molecule in the asymmetric unit ($Z' = 1$). There are no impurity phases observed in any of the SSNMR spectra. In agreement with numerical simulations, no noticeable splittings in the ^{13}C peaks is observed, demonstrating that adequate suppression of the effects of ^{14}N - ^{13}C residual dipolar coupling is achieved at 18.8 T.

The ^1H - ^{13}C CP/MAS spectra for cytosine and uracil are shown in Figures 1 and 2, respectively, along with simulated patterns used to determine the ^{13}C chemical shift tensors. The assignments, which were made on the basis of DFT calculations (vide infra), are shown in Scheme 1 and Table 1. For both compounds, the isotropic chemical shifts observed for the solids are similar to those for the same molecules dissolved in DMSO.⁸⁷ In the solid state, the values of δ_{iso} cover the range between 92.8 and 171.3 ppm, which is similar to other nitrogen-dense heterocyclic compounds.^{16,88–90} The chemical shift spans ($\Omega = \delta_{11} - \delta_{33}$) vary between 132.1 and 221.9 ppm, which is also representative of the ^{13}C chemical shift tensors of carbon atoms in nitrogen-dense heterocyclic compounds.^{16,88–90} Finally, we note that the ^{13}C chemical shift tensors for uracil have been previously measured at



SCHEME 1 Molecular structures and atomic labeling for the five nitrogen-dense organic compounds.

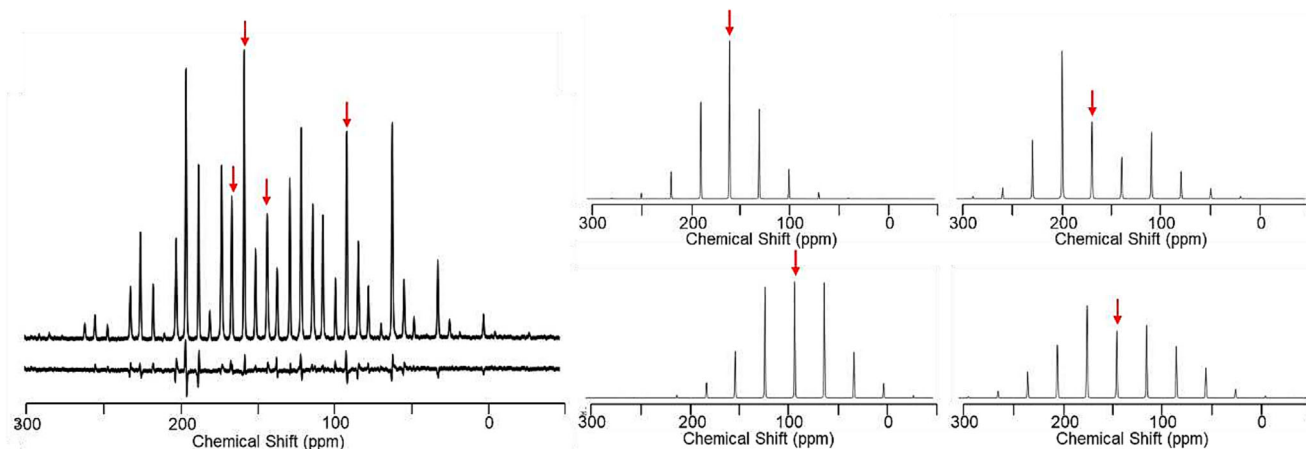


FIGURE 1 The ^1H - ^{13}C CP/MAS spectrum of cytosine (left side) acquired at 18.8 T with a spinning rate of $\nu_{\text{rot}} = 6.0$ kHz, along with simulated powder patterns for the four underlying carbon sites (right side). Red arrows indicate isotropic peak.

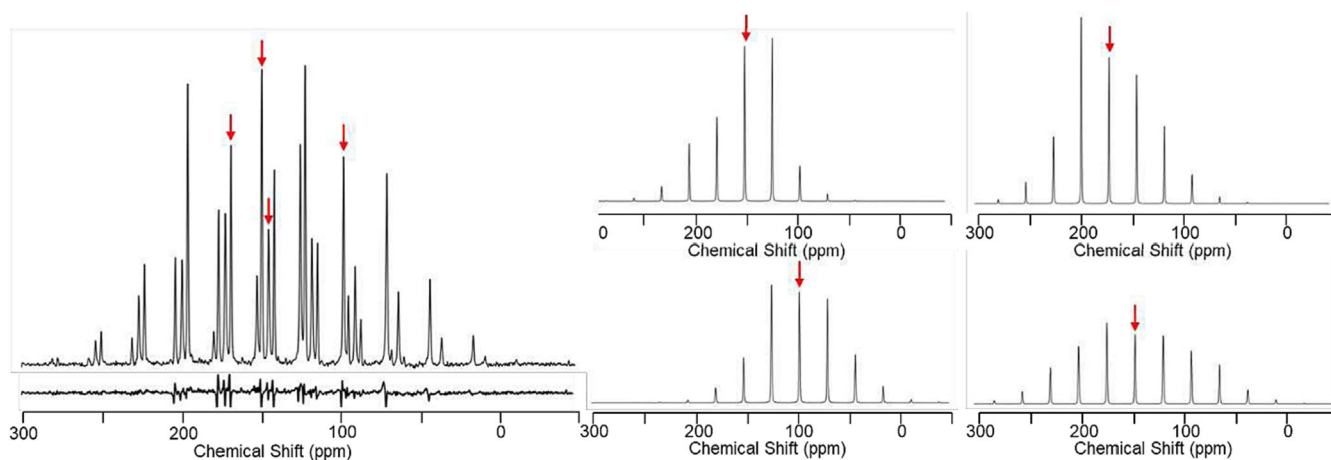


FIGURE 2 The $^1\text{H} \rightarrow ^{13}\text{C}$ CP/MAS spectrum of uracil (left side) acquired at 18.8 T with a spinning rate of $\nu_{\text{rot}} = 5.5$ kHz, along with simulated powder patterns for the four underlying carbon sites (right side). Red arrows indicate isotropic peak.

11.7 T⁴⁸, the values presented in the previous study are different from those herein (i.e., differences as large as 4.5 ppm are observed for different principal values, whereas the uncertainty in our experimental values are within ± 1.3 ppm), possibly reflecting the importance of high magnetic fields suppress the effects of ^{14}N - ^{13}C residual dipolar coupling.

The $^1\text{H} \rightarrow ^{13}\text{C}$ CP/MAS spectra for guanidine HCl, aminoguanidine HCl, and imidazole are shown in Figures S4–S6. Significantly, whereas the ^{13}C spectrum of imidazole in CDCl_3 indicates the presence of only two peaks⁸⁷ (due to the rapid exchange of protons), the solid-state spectrum indicates three, which is in agreement with the crystal structure. In contrast, the single isotropic peaks for guanidine HCl and aminoguanidine HCl are similar in the solid state and in D_2O .^{87,91} The chemical shift tensors observed for guanidine HCl and aminoguanidine HCl are remarkably similar, suggesting that long-range lattice effects have limited influence on these values.

We next compare the ^{13}C chemical shift tensors for these five compounds with those of seven additional molecules that contain nitrogen heterocycles. The number of ^{13}C chemical shift tensors for such systems is limited relative to other important chemical moieties, but includes the relevant carbon atoms in L-histidine HCl·H₂O, adenosine, cytidine, 2'-deoxythymidine, indigo, hypoxanthine, and cimetidine (i.e., 32 tensors altogether). In each case, we identify at least one previously reported ^{13}C chemical shift tensor that has a chemical shift distance of 10 ppm or less (i.e., $d_v \leq 10$ ppm), indicating the similarity of the principal values for the two tensors (Table S3). For cytosine, we find that the closest matches are for the four carbons atoms in cytidine, each of which features a value of $d_v \leq 4.3$ ppm. Similarly, for uracil, we find that the

closest matches are for carbons atoms in cytidine or 2'-deoxythymidine, although the values of d_v are larger in this case. Unsurprisingly, the ^{13}C chemical shift tensors for imidazole are most similar to those of other of atoms in imidazole groups, including atoms in L-histidine HCl·H₂O and cimetidine. Finally, guanidine HCl and aminoguanidine feature the largest values of d_v , indicating that the ^{13}C chemical shift tensors for guanidinium moieties are the most distinct from those of previously reported nitrogen heterocycles.

^{13}C magnetic shielding tensors for the five compounds were obtained from DFT calculations for comparison to the experimentally obtained ^{13}C chemical shift tensors (Figure 3). Four sets of calculation conditions are considered: The first set of calculations uses the GIPAW approach, combined with the GGA functional RPBE. The main advantage of the GIPAW method is that by satisfying the periodic boundary conditions, the plane-wave basis functions inherently account for the intermolecular interactions such as hydrogen bonding that may influence ^{13}C magnetic shielding tensors. However, such calculations are limited to the use of pure DFT functionals (e.g., LDA, GGA, and meta-GGA) due to the computational bottleneck associated with the combination of hybrid functionals and plane-wave basis sets.⁹² There are multiple methods for incorporating hybrid functionals into calculations, with one successful class involving the use of large clusters of molecules that account for lattice interactions.^{13–16} Furthermore, cluster-based structural models can be further augmented through use of electrostatic embedding techniques.^{17,42} As such, we employ two sets of calculations employing clusters with electrostatic embedding provided by the COSMO approach: The first set uses the GGA functional RPBE, whereas the second set uses the hybrid functional PBE0. These

TABLE 1 Experimental and calculated values for the ^{13}C chemical shift tensors for the five nitrogen-dense materials.

Compound	Position		δ_{iso} (ppm)	δ_{11} (ppm)	δ_{22} (ppm)	δ_{33} (ppm)
Guanidine HCl	1	Exp.	159.8	217.4(1.6)	192.9(1.3)	69.2(1.0)
		Calc.	155.0	204.0	194.2	66.9
Aminoguanidine HCl	1	Exp.	160.1	217.2(1.3)	193.2(1.0)	70.0(0.8)
		Calc.	157.4	205.9	202.0	64.2
Imidazole	1	Exp.	115.8	191.6(1.7)	118.3(1.2)	37.6(1.3)
		Calc.	117.2	196.9	117.6	37.1
	2	Exp.	127.4	200.9(1.8)	128.4(1.3)	52.8(1.4)
		Calc.	128.8	203.4	132.7	50.2
	3	Exp.	136.8	203.1(1.4)	146.3(1.0)	61.1(1.0)
		Calc.	139.0	204.1	153.1	59.9
Uracil	1	Exp.	151.8	228.7(0.6)	132.3(0.5)	94.5(0.4)
		Calc.	152.3	228.4	132.9	95.6
	2	Exp.	171.3	246.0(0.7)	181.6(0.5)	86.1(0.5)
		Calc.	170.6	244.5	180.5	86.7
	3	Exp.	100.2	175.7(1.3)	103.5(0.9)	21.2(1.0)
		Calc.	100.1	174.4	105.0	20.9
	4	Exp.	147.5	255.7(1.2)	152.9(0.8)	33.8(0.8)
		Calc.	150.9	261.1	158.7	33.0
Cytosine	1	Exp.	159.8	224.6(1.0)	162.4(0.7)	92.5(0.7)
		Calc.	160.4	223.1	165.2	92.8
	2	Exp.	168.1	240.2(1.4)	207.6(1.1)	56.5(0.9)
		Calc.	165.8	234.1	205.9	57.3
	3	Exp.	92.8	176.0(0.9)	91.6(0.7)	10.8(0.7)
		Calc.	92.3	174.3	90.7	11.9
	4	Exp.	144.8	248.8(0.7)	152.2(0.5)	33.5(0.5)
		Calc.	146.6	252.2	155.6	32.0

Note: The isotropic chemical shifts (δ_{iso}) are determined from separate $^1\text{H} \rightarrow ^{13}\text{C}$ CP/MAS spectra conducted with $\nu_{\text{rot}} = 10$ kHz, and is not necessary identical to the average of the three principal values of the chemical shift tensor (i.e., δ_{11} , δ_{22} , and δ_{33}). The chemical shift tensors are defined with the principal components ordered from highest to lowest frequency as $\delta_{11} \geq \delta_{22} \geq \delta_{33}$. Calculations were performed at the PBE0-DH/pc-3 level using the Monomer + Cluster + COSMO approach, as detailed in the main text. Uncertainties in the principal values reported in the parentheses are determined through HBA analysis.

calculations are denoted “Cluster + COSMO” method. Finally, it is sometimes desirable to explore the use of more modern functionals such as double-hybrid functionals (e.g., PBE0-DH), which have the potential to yield better agreement with experiment. Because of the large expense associated with high-level calculations, monomer corrections can be applied.^{20,22,23,43} Herein, the fourth set of calculations employs a monomer correction performed at the PBE0-DH level, applied to a cluster-based structural model with shielding tensors calculated with the PBE0 functional. The advantage of this method rests on the fact that magnetic shielding is largely a local phenomenon, meaning that the influences of weak non-covalent interactions on magnetic shielding tensors can

be calculated at a tractable lower level (i.e., PBE0 in this case). These calculations are denoted “Monomer + Cluster + COSMO” method. A summary of all calculated ^{13}C magnetic shielding tensors is provided in Table S4.

Statistical results for each set of calculations are provided in Table 2. Ideally, the conversion of ^{13}C magnetic shielding parameters to the chemical shift scale would feature a proportionality constant of $A = -1$ and a reference offset of $B = 186.4$ ppm (which was obtained from measurement of the spin-rotation constant of carbon monoxide).⁹³ However, Sherwood demonstrated that the correlation between predicted magnetic shielding and experimental chemical shift tensors could be improved

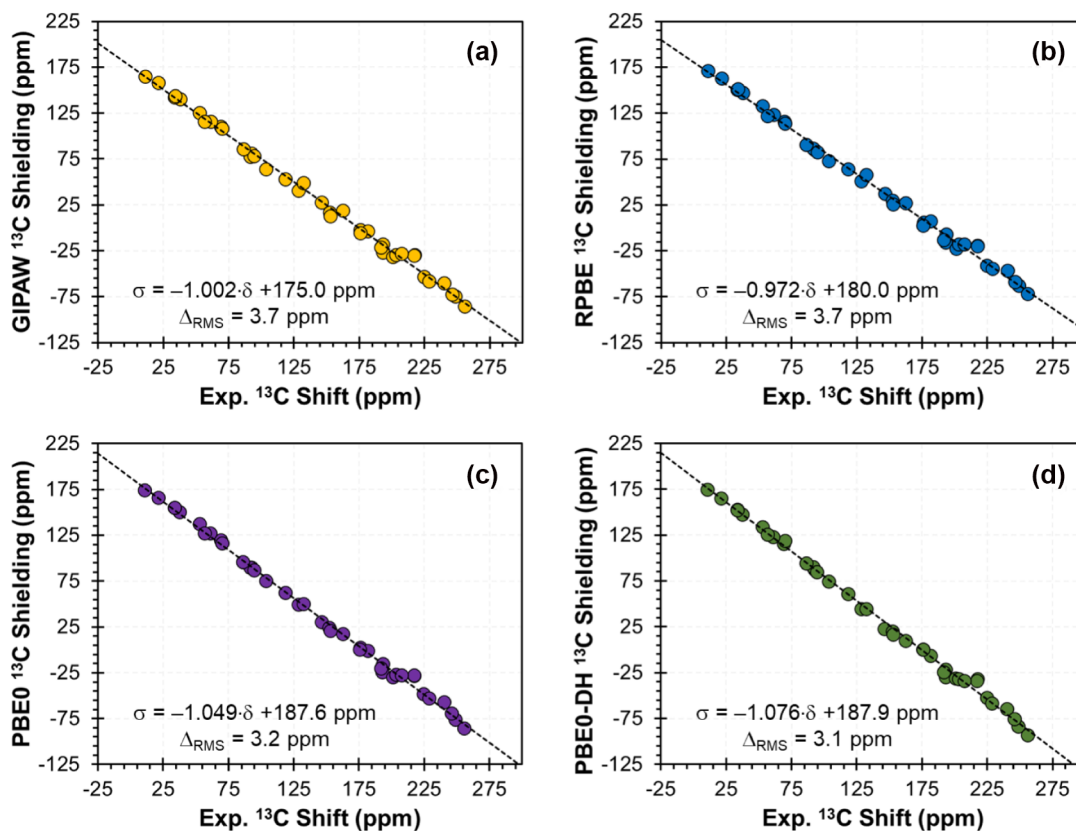


FIGURE 3 Correlations between calculated principal components of ^{13}C magnetic shielding tensors and experimental ^{13}C chemical shift tensors. Magnetic shielding tensors were computed following four protocols, as described in the main text: (a) the GIPAW method combined with the RPBE functional; (b) the Cluster + COSMO method combined with the RPBE functional; (c) the Cluster + COSMO method combined with the hybrid PBE0 functional; and (d) Monomer + Cluster + COSMO method, using a monomer correction at the double-hybrid PBE0-DH level, and the PBE0 for the cluster.

TABLE 2 Statistical results related to the correlations between calculated principal components of ^{13}C magnetic shielding tensors and experimental ^{13}C chemical shift tensors.

Method	Slope	Intercept (ppm)	Δ_{RMS} (ppm)
RPBE/GIPAW	-1.002	175.0	3.7
RPBE (Cluster + COSMO)	-0.972	180.0	3.7
PBE0 (Cluster + COSMO)	-1.049	187.6	3.2
PBE0-DH (Monomer + Cluster + COSMO)	-1.076	187.9	3.1

Note: The values of the slope (A) and intercept (B) of the correlation lines are defined in Equations S1 and S2, whereas errors in the calculations are provided by the RMS chemical shift distance (Δ_{RMS}), as defined in Equations S3 and S4.

by varying these parameters, to account for all types of systematic errors in the approach used to predict the shielding.⁹⁴ The values of A and B are typically obtained from linear least-squares regression²; however, in the present work, we optimize these values numerically with the goal of minimizing the value of the RMS chemical shift distance, Δ_{RMS} .

The results in Table 2 indicate that the agreement between calculation and experiment is strongly

influenced by the choice of functional used in the experiment. For example, both GIPAW and Cluster + COSMO calculations employing the functional RPBE result in comparatively large value of $\Delta_{\text{RMS}} = 3.7$ ppm. In contrast, Cluster + COSMO calculations employing the hybrid functional PBE0, and Monomer + Cluster + COSMO calculations employing the double-hybrid functional PBE0-DH, result in lower value of $\Delta_{\text{RMS}} = 3.2$ and 3.1 ppm, respectively. These values of Δ_{RMS} fall within

the range of the ^{13}C chemical shift tensors observed for other nitrogen-dense materials¹⁶ but somewhat larger than the typical values observed for the chemical shift tensors of saccharides and aromatic molecules,¹² demonstrating the importance of benchmarking quantum chemical calculations for the prediction of magnetic shielding tensors for atoms found in different chemical moieties.

Additionally, we have compared the calculated ^{13}C chemical shift tensors for uracil with the experimental values reported here and in previous work (Table S5).⁴⁸ These calculations were performed at the PBE0-DH level using the Monomer + Cluster + COSMO approach, because this method led to the best agreement with experiment overall (vide supra). We find that for each carbon atom, calculated values agree better with experiments performed at 18.8 T than those performed at 11.7 T (as indicated by the lower values of d_r for the ^{13}C chemical shift tensors reported in this work), demonstrating the synergy of high-level DFT calculations and SSNMR experiments for constructing a robust database of chemical shift tensors.

A key motivation for this work was to increase the number of accurately measured ^{13}C chemical shift tensors for nitrogen-dense compounds, along with performing high-level DFT calculations to model the relationships between experimental chemical shift tensors and calculated magnetic shielding tensors. Details related to three previous benchmarking studies were discussed in this work (vide supra) and are summarized as a histogram showing the distribution of the principal

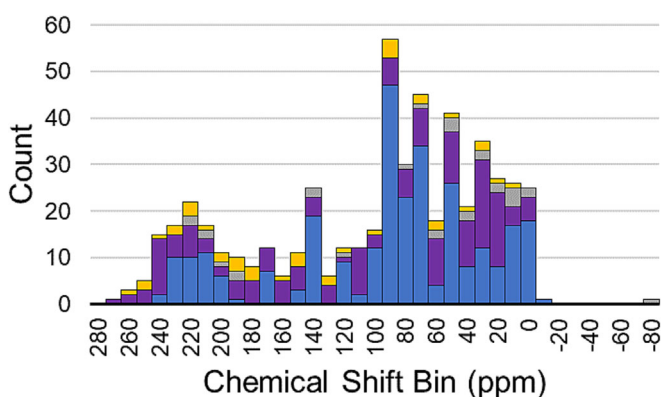


FIGURE 4 A histogram showing the number of principal values of ^{13}C chemical shift tensors featured in recent benchmark studies: the 2009 study by Johnston et al.¹² focusing on saccharides and aromatic compounds (blue); the 2014 study by Holmes et al.¹³ that added several amino acids, pharmaceuticals, and small molecules (purple); a 2020 study of the pharmaceutical cimetidine¹⁶ (gray); and the current work on nitrogen-dense compounds (yellow).

values of ^{13}C chemical shift tensors using a bin size of 10 ppm (Figure 4). This histogram shows how the present measurements augment the chemical shift tensor principal values for underrepresented chemical moieties with a wide range of chemical shift principal values, which is a critical consideration for establishing a database suitable for rigorous benchmarking.

4 | CONCLUSIONS

The ^{13}C chemical shift tensors for five nitrogen-dense organic molecular solids have been measured at a field strength of 18.8 T. Use of a high field proved to be beneficial because the effects of ^{14}N - ^{13}C residual dipolar coupling are minimized, allowing the ^{13}C chemical shift tensor parameters to be determined from relative sideband intensities. Furthermore, a series of DFT calculations were performed to assign the ^{13}C peaks in each system and to benchmark the performance of various DFT protocols for predicting ^{13}C magnetic shielding tensors for materials with an abundance of carbon–nitrogen bonds, as comparatively large errors for such systems have been reported.¹⁶ The best agreement with experiment is obtained from calculations using the hybrid functional PBE0 or the double-hybrid functional PBE0-DH, along with the triple-zeta basis sets TZ2P or pc-3, respectively, and intermolecular effects modeled using large clusters of molecules with electrostatic embedding through the COSMO approach. These measurements are part of an ongoing effort to expand the catalog of accurate ^{13}C chemical shift tensor measurements, which may prove useful for researchers that wish to characterize APIs or other biologically relevant nitrogen-dense materials featuring carbon–nitrogen bonds and contribute toward building a robust database of ^{13}C chemical shift tensors that will aid NMR crystallographic endeavors.

This project provided a unique and far-reaching experience for undergraduate research students, who were involved in preparing samples for SSNMR experiments, acquiring $^1\text{H} \rightarrow ^{13}\text{C}$ SSNMR spectra for relatively challenging samples, simulating the spectra for the determination of ^{13}C chemical shift tensor parameters, and conducting first-principles quantum chemical computations. The framework of this project could be extended for larger groups of undergraduate researchers in the future, as there is a clear necessity for increasingly accurate measurements and calculations of ^{13}C chemical shift tensors.

ACKNOWLEDGMENTS

R.W.S. is grateful for support from The Florida State University and the National High Magnetic Field

Laboratory, which is funded by the National Science Foundation Cooperative Agreement (DMR-1644779, DMR-2128556), and the State of Florida. R.J.I. acknowledges support from MRI CHE-1726824 and REU CHE-1950585. A portion of this research used resources provided by the X-ray Crystallography Center at the FSU Department of Chemistry and Biochemistry (FSU075000XRAY). The undergraduate researchers, R.J.I., and R.W.S are very grateful to the NHMFL for support of the Winter NMR School and travel funds.

PEER REVIEW

The peer review history for this article is available at <https://www.webofscience.com/api/gateway/wos/peer-review/10.1002/mrc.5422>.

ORCID

Robert W. Schurko  <https://orcid.org/0000-0002-5093-400X>

REFERENCES

- [1] J. C. Facelli, *Prog Nucl Magn Reson Spectrosc* **2011**, *58*, 176.
- [2] D. W. Alderman, M. H. Sherwood, D. M. Grant, *J Magn Reson* **1993**, *101*, 188.
- [3] M. A. Kennedy, P. D. Ellis, *Concepts Magn Reson* **1989**, *1*, 35.
- [4] M. A. Kennedy, P. D. Ellis, *Concepts Magn Reson* **1989**, *1*, 109.
- [5] T. Vosegaard, *Prog Nucl Magn Reson Spectrosc* **2021**, *123*, 51.
- [6] J. K. Harper, R. J. Iulucci, C-13 chemical shift tensors in organic materials, in *Encyclopedia of Analytical Chemistry*, John Wiley & Sons, Ltd., New York City, USA **2014**. <https://doi.org/10.1002/9780470027318.a9295>
- [7] F. Taulelle, *Solid State Sci* **2004**, *6*, 1053.
- [8] R. K. Harris, R. E. Wasylshen, *NMR Crystallography*, Wiley-VCH Verlag **2018**.
- [9] P. Hodgkinson, *Prog Nucl Magn Reson Spectrosc* **2020**, *118–119*, 10.
- [10] C. Martineau, *Solid State Nucl Magn Reson* **2014**, *63–64*, 1.
- [11] D. L. Bryce, *IUCrJ* **2017**, *4*, 350.
- [12] J. C. Johnston, R. J. Iulucci, J. C. Facelli, G. Fitzgerald, K. T. Mueller, *J Chem Phys* **2009**, *131*, 144503. <https://doi.org/10.1063/1.3225270>
- [13] S. T. Holmes, R. J. Iulucci, K. T. Mueller, C. Dybowski, *J Chem Phys* **2014**, *141*(164), 121.
- [14] S. T. Holmes, R. J. Iulucci, K. T. Mueller, C. Dybowski, *J Chem Theory Comput* **2015**, *11*, 5229.
- [15] F. Alkan, S. T. Holmes, C. Dybowski, *J Chem Theory Comput* **2017**, *13*, 4741.
- [16] S. T. Holmes, O. G. Engl, M. N. Srncic, J. D. Madura, R. Quiñones, J. K. Harper, R. W. Schurko, R. J. Iulucci, *J Phys Chem A* **2020**, *124*, 3109.
- [17] J. D. Hartman, A. Balaji, G. J. O. Beran, *J Chem Theory Comput* **2017**, *13*, 6043.
- [18] J. D. Hartman, G. J. O. Beran, *J Chem Theory Comput* **2014**, *10*, 4862.
- [19] J. D. Hartman, G. M. Day, G. J. O. Beran, *Cryst Growth Des* **2016**, *16*, 6479.
- [20] J. D. Hartman, J. K. Harper, *Solid State Nucl Magn Reson* **2022**, *122*, 101832.
- [21] J. D. Hartman, R. A. Kudla, G. M. Day, L. J. Mueller, G. J. O. Beran, *Phys Chem Chem Phys* **2016**, *18*, 21686.
- [22] M. Dračinský, P. Unzueta, G. J. O. Beran, *Phys Chem Chem Phys* **2019**, *21*, 14992.
- [23] R. J. Iulucci, J. D. Hartman, G. J. O. Beran, *J Phys Chem A* **2023**, *127*, 2846.
- [24] S. E. Ashbrook, D. McKay, *Chem Commun* **2016**, *52*, 7186.
- [25] C. Bonhomme, C. Gervais, F. Babonneau, C. Coelho, F. Pourpoint, T. Azaïs, S. E. Ashbrook, J. M. Griffin, J. R. Yates, F. Mauri, et al., *Chem Rev* **2012**, *112*, 5733.
- [26] S. T. Holmes, W. D. Wang, G. Hou, C. Dybowski, W. Wang, S. Bai, *Phys Chem Chem Phys* **2019**, *21*, 6319.
- [27] J. K. Harper, D. M. Grant, *Cryst Growth Des* **2006**, *6*, 2315.
- [28] K. Kalakewich, R. Iulucci, J. K. Harper, *Cryst Growth Des* **2013**, *13*, 5391.
- [29] J. K. Harper, D. H. Barich, E. M. Heider, D. M. Grant, R. R. Franke, J. H. Johnson, Y. Zhang, P. L. Lee, R. B. Von Dreele, B. Scott, et al., *Cryst Growth Des* **2005**, *5*, 1737.
- [30] J. K. Harper, J. A. Doebbler, E. Jacques, D. M. Grant, R. B. Von Dreele, *J Am Chem Soc* **2010**, *132*, 2928.
- [31] J. K. Harper, D. M. Grant, Y. Zhang, P. L. Lee, R. Von Dreele, *J Am Chem Soc* **2006**, *128*, 1547.
- [32] C. Yang, L. Zhu, R. A. Kudla, J. D. Hartman, R. O. Al-Kaysi, S. Monaco, B. Schatschneider, A. Magalhães, G. J. O. Beran, C. J. Bardeen, et al., *CrystEngComm* **2016**, *18*, 7319.
- [33] D. V. Dudenko, P. A. Williams, C. E. Hughes, O. N. Antzutkin, S. P. Velaga, S. P. Brown, K. D. M. Harris, *J Phys Chem C* **2013**, *117*, 12258.
- [34] C. J. H. Smalley, H. E. Hoskyns, C. E. Hughes, D. N. Johnstone, T. Willhammar, M. T. Young, C. J. Pickard, A. J. Logsdail, P. A. Midgley, K. D. M. Harris, *Chem Sci* **2022**, *13*, 5277.
- [35] K. D. M. Harris, *Crystals* **2022**, *12*, 1277.
- [36] P. A. Unzueta, C. S. Greenwell, G. J. O. Beran, *J Chem Theory Comput* **2021**, *17*, 826.
- [37] J. B. Kleine Büning, S. Grimme, *J Chem Theory Comput* **2023**, *19*, 3601.
- [38] M. Cordova, E. A. Engel, A. Stefaniuk, F. Paruzzo, A. Hofstetter, M. Ceriotti, L. Emsley, *J Phys Chem C* **2022**, *126*, 16710.
- [39] F. M. Paruzzo, A. Hofstetter, F. Musil, S. De, M. Ceriotti, L. Emsley, *Nat Commun* **2018**, *9*, 4501.
- [40] H. Sun, S. Dwaraknath, H. Ling, X. Qu, P. Huck, K. A. Persson, S. E. Hayes, *Npj Comput Mater* **2020**, *6*, 53.
- [41] C. J. Pickard, F. Mauri, *Phys Rev B* **2001**, *63*, 245101.
- [42] P. A. Unzueta, G. J. O. Beran, *J Comput Chem* **2020**, *41*, 2251.
- [43] T. Nakajima, *Chem Phys Lett* **2017**, *677*, 99.
- [44] R. K. Harris, A. C. Olivieri, *Prog Nucl Magn Reson Spectrosc* **1992**, *24*, 435.
- [45] M. Strohmeier, D. W. Alderman, D. M. Grant, *J Magn Reson* **2002**, *155*, 263.
- [46] M. Strohmeier, D. Stueber, D. M. Grant, *J Phys Chem A* **2003**, *107*, 7629.
- [47] M. Strohmeier, D. M. Grant, *J Am Chem Soc* **2004**, *126*, 966.
- [48] S. K. Amini, H. Shaghghi, A. D. Bain, A. Chabok, M. Tafazzoli, *Solid State Nucl Magn Reson* **2010**, *37*, 13.
- [49] D. L. Barker, R. E. Marsh, *Acta Crystallogr* **1964**, *17*, 1581.

- [50] R. F. Stewart, L. H. Jensen, *Acta Crystallogr* **1967**, *23*, 1102.
- [51] D. J. Haas, D. R. Harris, H. H. Mills, *Acta Crystallogr* **1965**, *19*, 676.
- [52] J. H. Bryden, *Acta Crystallogr* **1957**, *10*, 677.
- [53] G. Will, *Z Kristallogr* **1969**, *129*, 211.
- [54] P. L. Gor'kov, E. Y. Chekmenev, C. Li, M. Cotten, J. J. Buffy, N. J. Traaseth, G. Veglia, W. W. Brey, *J Magn Reson* **2007**, *185*, 77.
- [55] O. B. Peersen, X. L. Wu, I. Kustanovich, S. O. Smith, *J Magn Reson, Ser A* **1993**, *104*, 334.
- [56] G. Metz, X. L. Wu, S. O. Smith, *J Magn Reson, Ser A* **1994**, *110*, 219.
- [57] J. Schaefer, E. O. Stejskal, *J Am Chem Soc* **1976**, *98*, 1031.
- [58] A. Pines, J. S. Waugh, M. G. Gibby, *Chem Phys Lett* **1972**, *15*, 373.
- [59] A. Pines, M. G. Gibby, J. S. Waugh, *J Chem Phys* **1973**, *11*, 569.
- [60] B. M. Fung, A. K. Khitrin, K. Ermolaev, *J Magn Reson* **2000**, *142*, 97.
- [61] S. R. Hartmann, E. L. Hahn, *Phys Rev* **1962**, *128*, 2042.
- [62] M. J. Potrzebowski, P. Tekely, Y. Dusausoy, *Solid State Nucl Magn Reson* **1998**, *11*, 253.
- [63] R. E. Taylor, *Concepts Magn Reson* **2004**, *22A*, 37.
- [64] S. G. J. van Meerten, W. M. J. Franssen, A. P. M. Kentgens, *J Magn Reson* **2019**, *301*, 56.
- [65] K. Eichele, *HBA: Herzfeld-Berger Analysis Program (Version 1.8.1)*, Universität Tübingen, Tübingen, Germany **2021**.
- [66] K. Eichele, *WSOLIDS1: Solid-State NMR Simulation (Version 1.21.7)*, Universität Tübingen, Tübingen, Germany **2021**.
- [67] S. J. Clark, M. D. Segall, C. J. Pickard, P. J. Hasnip, M. J. Probert, K. Refson, M. C. Payne, *Z Kristallogr* **2005**, *220*, 567.
- [68] B. Hammer, L. B. Hansen, J. K. Nørskov, *Phys Rev B* **1999**, *59*, 7413.
- [69] J. R. Yates, C. J. Pickard, F. Mauri, *Phys Rev B* **2007**, *76*, 024401.
- [70] H. J. Monkhorst, J. D. Pack, *Phys Rev B* **1976**, *13*, 5188.
- [71] S. Grimme, *J Comput Chem* **2006**, *27*, 1787.
- [72] B. G. Pfrommer, M. Côté, S. G. Louie, M. L. Cohen, *J Comput Phys* **1997**, *131*, 233.
- [73] R. Ditchfield, *Mol Phys* **1974**, *27*, 789.
- [74] K. Wolinski, J. F. Hinton, P. Pulay, *J Am Chem Soc* **1990**, *112*, 8251.
- [75] C. Adamo, V. Barone, *J Chem Phys* **1999**, *110*, 6158.
- [76] A. D. Becke, *J Chem Phys* **1988**, *88*, 2547.
- [77] M. Franchini, P. H. T. Philipsen, L. Visscher, *J Comput Chem* **2013**, *34*, 1819.
- [78] A. Klamt, G. Schüürmann, *J Chem Soc, Perkin Trans* **1993**, *2*, 799.
- [79] A. Klamt, *J Phys Chem* **1995**, *99*, 2224.
- [80] A. Klamt, V. Jonas, *J Chem Phys* **1996**, *105*, 9972.
- [81] A. Klamt, C. Moya, J. Palomar, *J Chem Theory Comput* **2015**, *11*, 4220.
- [82] C. C. Pye, T. Ziegler, *Theor Chem Acc* **1999**, *101*, 396.
- [83] B. Delley, *Mol Sim* **2006**, *32*, 117.
- [84] N. L. Allinger, X. Zhou, J. Bergsma, *J Mol Struct (THEOCHEM)* **1994**, *312*, 69.
- [85] E. Brémond, C. Adamo, *J Chem Phys* **2011**, *135*, 024106.
- [86] F. Jensen, *J Chem Phys* **2001**, *115*, 9113.
- [87] ChemicalBook. ChemicalBook. (accessed 15 Aug 2023).
- [88] D. Stueber, D. M. Grant, *J Am Chem Soc* **2002**, *124*, 10539.
- [89] K. Maliňáková, L. Novosadová, M. Lahtinen, E. Kolehmainen, J. Brus, R. Marek, *J Phys Chem A* **2010**, *114*, 1985.
- [90] S. T. Holmes, C. Dybowski, *Solid State Nucl Magn Reson* **2015**, *72*, 90.
- [91] SpectraBase. Wiley Science Solutions. (accessed 15 Aug 2023).
- [92] P. Broqvist, A. Alkauskas, A. Pasquarello, *Phys Rev B* **2009**, *80*, 085114.
- [93] A. K. Jameson, C. J. Jameson, *Chem Phys Lett* **1987**, *134*, 461.
- [94] M. H. Sherwood, J. C. Facelli, D. W. Alderman, D. M. Grant, *J Am Chem Soc* **1991**, *113*, 750.

SUPPORTING INFORMATION

Additional supporting information can be found online in the Supporting Information section at the end of this article.

How to cite this article: S. T. Holmes, C. M. Boley, A. Dewicki, Z. T. Gardner, C. S. Vojvodin, R. J. Iuliucci, R. W. Schurko, *Magn Reson Chem* **2024**, *62*(3), 179. <https://doi.org/10.1002/mrc.5422>